HHS Public Access

Author manuscript

J Bone Miner Res. Author manuscript; available in PMC 2017 June 01.

Published in final edited form as:

J Bone Miner Res. 2016 June ; 31(6): 1247–1257. doi:10.1002/jbmr.2792.

Conditional Deletion of Murine Fgf23: Interruption of the Normal Skeletal Responses to Phosphate Challenge and Rescue of Genetic Hypophosphatemia

Erica L. Clinkenbeard[1], **Taryn A. Cass**[1], **Pu Ni**[1], **Julia M. Hum**[1], **Teresita Bellido**[2], **Matthew R. Allen**[2], and **Kenneth E. White**[1,*]

[1]Department of Medical and Molecular Genetics, Indiana University School of Medicine, Indianapolis, IN, USA

[2]Department of Anatomy and Cell Biology, Indiana University School of Medicine, Indianapolis, IN, USA

Abstract

The transgenic and knock out (KO) animals involving *Fgf23* have been highly informative in defining novel aspects of mineral metabolism, but are limited by shortened life span, inability of spatial/temporal FGF23 control, and infertility of the global KO. To more finely test the role of systemic and genetic influences in FGF23 production, a mouse was developed that carried a floxed ('f')-*Fgf23* allele (exon 2 floxed) which demonstrated in vivo recombination when bred to global-Cre transgenic mice (*eIIa*-cre). Mice homozygous for the recombined allele ('Δ') had undetectable serum intact FGF23, elevated serum phosphate ($p<0.05$), and increased kidney Cyp27b1 mRNA ($p<0.05$) similar to global *Fgf23*-KO mice. To isolate cellular FGF23 responses during phosphate challenge $Fgf23^{\Delta/f}$ mice were mated with early osteoblast type Iα1 collagen 2.3kb promoter-cre mice (Col2.3-cre) and the late osteoblast/early osteocyte Dentin matrix protein-1-cre (Dmp1-cre). $Fgf23^{\Delta/f}$/Col2.3-cre^{+} and $Fgf23^{\Delta/f}$/Dmp1-cre^{+} exhibited reduced baseline serum intact FGF23 versus controls. After challenge with high phosphate diet Cre^{-} mice had 2.1–2.5 fold increased serum FGF23 ($p<0.01$), but Col2.3-cre^{+} mice had no significant increase, and Dmp1-cre^{+} mice had only a 37% increase ($p<0.01$) despite prevailing hyperphosphatemia in both models. The $Fgf23^{\Delta/f}$/Col2.3-cre was bred onto the *Hyp* (murine XLH model) genetic background to test the contribution of osteoblasts and osteocytes to elevated FGF23 and *Hyp* disease phenotypes. Whereas *Hyp* mice maintained inappropriately elevated FGF23 considering their marked hypophosphatemia, *Hyp*/$Fgf23^{\Delta/f}$/Col2.3-cre^{+} mice had serum FGF23 <4% of *Hyp* ($p<0.01$), and this targeted restriction normalized serum phosphorus and ricketic bone disease. In summary, deleting FGF23 within early osteoblasts and osteocytes demonstrated that both cell types

*Corresponding author information: Kenneth E. White, Ph.D., Department of Medical & Molecular Genetics, Indiana University School of Medicine, 975 West Walnut St., IB130, Indianapolis, IN 46202, Office phone: (317) 278-1775, Fax: (317) 274-2293, ; Email: kenewhit@iupui.edu

Author's roles: ELC and KEW contributed to the study design. ELC, TAC, PN, JMH and MRA collected and analyzed data, TB provided critical reagents/mouse. ELC, MRA, TB and KEW wrote, and critically revised the final draft of the manuscript.

The other authors have no conflicts.

Disclosures

KEW receives royalties for licensing the FGF23 gene to Kyowa-Hakko-Kirin Pharmaceutics, Inc. and receives funding from Eli Lilly & Co.

contribute to baseline circulating FGF23 concentrations, and that targeting osteoblasts/osteocytes for FGF23 production can modify systemic responses to changes in serum phosphate concentrations and rescue the *Hyp* genetic syndrome.

Keywords

FGF-23; Klotho; phosphate; XLH; osteoblast; osteocyte; vitamin D; cre-recombinase

Introduction

Phosphate is central to basic cellular functions and is essential for proper mineralization of bone, therefore blood phosphate concentrations are maintained within a fairly narrow range. Serum phosphate levels are controlled by a balance of endocrine effects on intestinal uptake from the diet, coupled with renal handling and storage in bone ([1]). Fibroblast growth factor-23 (FGF23) is a key hormone involved in maintaining phosphate balance, primarily through control of renal phosphate reabsorption ([2]). In kidney, FGF23 interacts with its co-receptor αKlotho (αKL) and an FGF receptor (FGFR) to activate the MAPK pathway ([3, 4]). These interactions decrease expression of the renal proximal tubule sodium phosphate cotransporters NPT2a and NPT2c, responsible for renal phosphate reabsorption ([5, 6]). In parallel, serum $1,25(OH)_2$ vitamin D (1,25D) is reduced through FGF23-dependent down regulation of the anabolic 1α-hydroxylase (*CYP27b1*), and increased catabolic enzyme 24-hydroxylase (*CYP24a1*) expression ([5]). FGF23 is primarily produced in bone ([7]), and FGF23 mRNA and circulating concentrations are influenced by multiple factors including systemic changes in phosphate ([8]), 1,25D ([9, 10]), PTH ([11]), iron handling ([12]), as well as local factors including FGF/FGFR1 signaling ([13, 14]). Although thought to be primarily produced in osteocytes, which cells in bone are the source(s) of FGF23, as well as the mechanisms directing the ability of bone cells to produce FGF23 downstream of the aforementioned factors remain unclear.

Several heritable and acquired metabolic bone diseases are caused by disturbances in FGF23. In this regard, an increase in circulating bioactive FGF23 is associated with autosomal dominant hypophosphatemic rickets (ADHR) ([15]), autosomal recessive hypophosphatemic rickets type 1–3 (ARHR1: mutations in *DMP1*; ARHR2: mutations in *ENPP1*; and ARHR3: mutations in *FAM20C* (Raine syndrome) ([16–19])), X-linked hypophosphatemic rickets (XLH) ([20]), as well as tumor induced osteomalacia (TIO) ([5, 20]). Although these syndromes have heterogeneous genetic causes, they share a common phenotype of elevated FGF23, leading to hypophosphatemia secondary to renal phosphate wasting with inappropriately low or normal serum 1,25D. The reciprocal disorder to ADHR, familial hyperphosphatemic tumoral calcinosis (hFTC), is caused by loss of function mutations in *FGF23* ([21, 22]), the *O*-glycosylating enzyme *GALNT3* ([23]), and *αKL* ([24]). The *GALNT3* and *FGF23* mutations result in destabilized FGF23 protein and thus low circulating intact hormone ([25, 26]). End organ resistance to serum FGF23 is the likely cause of the severe hyperphosphatemia due to *αKL* inactivating mutations observed in humans ([24]) and in the global *αKl* knock-out (KO) mice ([4]). The mouse models of transgenic FGF23 excess ([6, 27]) and global *Fgf23*-KO ([28, 29]) have been useful in determining some

of the molecular mechanisms underlying genetic diseases resulting from alterations in FGF23 bioactivity. These models have proven to phenocopy the majority of the key phenotypes in aforementioned diseases of FGF23 excess and reduction. However, the cellular mechanisms and localization of FGF23 production during changes in serum phosphate and in genetic disorders involving FGF23 are unknown. Additionally, the currently available animal models are characterized by severe endocrine and skeletal manifestations and are therefore limited by shortened life span, inability of spatial and temporal FGF23 control, and infertility of the global *Fgf23*-KO ([6, 27–30]).

To more finely examine FGF23 expression and function *in vivo*, a mouse harboring a conditional *Fgf23* allele (flox-*Fgf23*) was developed. With osteoblast/osteocyte lineage-specific recombination, conditional-null *Fgf23* mice had suppressed circulating intact FGF23 that was resistant to normal responses to phosphate challenge. Further, when bred onto the genetic background of the XLH mouse model *Hyp*, characterized by an osteoblast differentiation defect and aberrant FGF23 production despite prevailing hypophosphatemia, the recombined *Fgf23* allele rescued hallmark endocrine and skeletal disease phenotypes. These findings support that osteocytes and osteoblasts control baseline circulating FGF23, and that targeting osteoblast/osteocyte FGF23 disrupts normal systemic responses to changes in phosphate handling.

Materials and Methods

Animal studies

Animal studies were approved by and performed according to the Institutional Animal Care and Use Committee (IACUC) for Indiana University, and comply with the NIH guidelines for the use of animals in research. Flox-*Fgf23* mice were derived as described immediately below and *Hyp* mice were purchased as live stock (JAX; Bar Harbor, ME). In *Hyp* studies, littermates were injected with calcein (10 mg/kg) at 7 days, then alizarin red (20 mg/kg) at 2 days, prior to necropsy and tissue harvest according to standard protocols.

Generation of a conditional Fgf23 allele

Exon 2 of the mouse *Fgf23* gene was targeted for Cre-mediated recombination, since deletion of this exon is predicted to result in a truncation of FGF23 protein (Supplemental Figure 1). To this end, a 9.4 kb target region of mouse *Fgf23* identified from BAC clone RP23:142M1 was subcloned into the pSP72 backbone plasmid. A single LoxP site was inserted downstream of exon 2. The 1.7 kb pGK-gb2 LoxP/FRT-flanking Neomycin cassette (Neo^R) was inserted upstream of exon 2, which contained new *BamHI* and *NcoI* restriction sites. Restriction enzyme digests and sequencing confirmed the final targeting vector (depicted in Supplemental Figure 2). The targeting vector was separated from the vector backbone with *NotI* and injected into BA1 ES cells. Positive ES cell clones were identified with G418 selection, and homologous recombination events within the *Fgf23* locus (Supplemental Figure 2) were confirmed with PCR and Southern blotting (Supplemental Figure 2). ES cell DNA were digested with *NcoI* and probed with a 462 bp 3′-external probe for long arm recombination. DNA digested with *BamHI* and probed with a 515 bp 5′-

internal probe confirmed short arm homologous recombination (Supplemental Figure 2) as designed by InGenious, Inc. (Ronkonkoma, NY).

Conditional deletion of Fgf23 in mice

Chimeric mice were mated to the FLP-Cre transgenic mice (C57BL/6 FLP: stock#005703; JAX, Bar Harbor, ME) to simultaneously assess germline transmission and delete the FRT-neomycin resistance (Neo^R) cassette, confirmed through PCR genotyping. The F1-generation heterozygous flox-*Fgf23* (*Fgf23*$^{f/+}$) mice were either intercrossed to generate homozygous flox (*Fgf23*$^{f/f}$) mice, or bred to generate *Fgf23*$^{f/+}$/$Cre^{+/-}$ and *Fgf23*$^{\Delta/+}$ (Δ=recombined *Fgf23* allele) mice using the *eIIa*-cre (JAX), the 2.3kb promoter rat type Iα1 collagen-cre (Col2.3-cre) ([31]), and the 8kb-Dentin matrix protein 1 (Dmp1)-cre ([32]) mouse lines. *Fgf23*$^{\Delta/f}$ littermates positive or negative for the appropriate transgenic Cre were used for subsequent analysis. For analysis of phenotypes arising from matings between *Hyp* and *Fgf23*-flox mice, controls labeled as '*Hyp*' were genotyped as carrying the known *Hyp Phex* 3′ deletion ([33]) with at least one wild type ('+') *Fgf23* allele, or carry at least one floxed-*Fgf23* allele (*Fgf23*^{f}) and are Cre^{-}: *Hyp*/*Fgf23*$^{\Delta/f}$/Col2.3-cre^{-}, *Hyp*/*Fgf23*$^{f/+}$/Col2.3-$cre^{+/-}$, and *Hyp*/*Fgf23*$^{\Delta/+}$/Col2.3-cre^{+}. For comparisons, phenotypically normal littermate mice were wild type for *Phex* and genotyped as *Fgf23*$^{\Delta/+}$/Col2.3-cre^{+}, *Fgf23*$^{\Delta/f}$/Col2.3-cre^{-}, or *Fgf23*$^{f/f}$/Col2.3-cre^{-}.

Rodent diets

Mice were weaned at three weeks of age and maintained until euthanasia at 8 weeks on a standard rodent diet (0.7% phosphate and 1.0% calcium, Harlan-Teklad, Inc.; Madison, WI). To induce FGF23 production littermates were placed on a high phosphate ('HighP') diet containing 1.65% phosphate and 1.0% calcium (Diet #TD 88345; Harlan-Teklad), from 6 weeks of age for 2 weeks. Diets and water were provided ad libitum throughout the experimental time frames.

Serum biochemistries

Blood samples were collected from mice at the time of euthanasia by cardiac puncture, or for interim analyses by facial vein bleed according to approved protocols. Routine serum biochemistries were determined in the Laboratory of the Clinical and Translational Sciences Institute (CTSI) of the Indiana University School of Medicine using an automated COBAS MIRA Plus Chemistry Analyzer (Roche Diagnostics; Indianapolis, IN), or using the Inorganic Phosphorous Reagent kit (Pointe Scientific, Inc.; Brussels, Belgium). Serum 'intact' FGF23, and 'total or *C*-terminal' FGF23 concentrations were assessed using commercial ELISAs (Kainos Laboratories Int'l; Tokyo, Japan (intact); or Immutopics, Int'l; San Clemente, CA (intact and *C*-terminal)). Serum intact PTH was measured using commercial ELISA (Immutopics Int'l.).

Micro-computed tomography (μCT)

Femurs were removed post-necropsy and fixed in 4% PFA. Bones were scanned using μCT (Skyscan 1172), at 6 micron resolution, to assess trabecular and cortical bone morphometry. A defined region of interest in the distal femur (~0.5 mm from the growth plate and

encompassing 1 mm of slices in the proximal direction) was used to determine trabecular bone volume/total volume (BV/TV). A single cortical bone slice (2 mm proximal to the above region of interest) was analyzed for cortical geometry. The terminology and units used are those recommended by the American Society for Bone and Mineral Research Guidelines for assessment of bone microstructure in rodents using μCT ([34]).

Histomophometric analyses

Following μCT analysis, bones were embedded in methyl methacrylate using standard protocols. Mid-sagittal (4 μm) sections of cancellous bone from the distal femur and transverse (~100 μm) sections of the mid-diaphysis were cut using a microtome (Reichert-Jung 2050 Supercut; Leica Microsystems, Buffalo Grove, IL) and wire-saw (Histosaw; Delaware Diamond Knives), respectively. The cancellous sections were stained with von Kossa tetrachrome according to established protocols. Diaphysis sections were ground to roughly 40 μm thickness. Periosteal and endocortical dynamic bone parameters were obtained using a semi- automatic analysis system (Bioquant OSTEO; Bioquant Image Analysis Co.) attached to a Nikon microscope. The terminology and units used are those recommended by the Histomorphometry Nomenclature Committee of the American Society for Bone and Mineral Research ([35]).

RNA preparation and quantitative RT-PCR (qPCR)

Kidneys were harvested and homogenized in 1 mL of Trizol reagent (Invitrogen/Life Technologies, Inc.; Grand Island, NY) according to the manufacturer's protocol using a TissueTearor rotor-stator (Biospec Products, Inc.; Bartlesville, OK), then further purified using the RNeasy Kit (Qiagen, Inc.; Germantown, MD). RNA samples were tested with intron-spanning primers specific for *Fgf23*, and vitamin D 1α-hydroxylase (*Cyp27b1*) mRNAs; mouse *β-actin* was used as an internal control. The qPCR primers and probes were purchased as pre-optimized reagents (Applied Biosystems/Life Technologies, Inc.). The TaqMan One-Step RT-PCR kit was used to perform qPCR. PCR conditions for all experiments were: 30 min 48°C, 10 min 95°C, followed by 40 cycles of 15 sec 95°C and 1 min 60°C. The data was collected and analyzed by a 7500 Real Time PCR or StepOne Plus systems (Applied Biosystems/Life Technologies, Inc.). The expression levels of mRNAs were calculated relative to appropriate littermate genotype controls, and the $2^{-\Delta\Delta CT}$ method described by Livak was used to analyze the data ([36]).

DNA sequencing

Sequencing of genomic DNA following *ella*-cre-mediated recombination of the flox-*Fgf23* alleles was performed using standard PCR (KOD DNA Polymerase; EMD-Millipore, Inc.) to generate gene fragments followed by Exosap (Affymetrix, Inc.; Santa Clara, CA) preparation of templates. Dideoxysequencing was carried out on the genomic fragments by a commercial vendor (SeqWright Genomic Services; Houston, TX) using the forward or reverse PCR primers.

Statistical analysis

Statistical analysis of the in vivo and in vitro data was performed by one-way ANOVA followed by a Tukey post-hoc test and Student's *t*-test, respectively. Significance for all tests was set at $p<0.05$. Data are presented as means ± standard error of the mean (SEM).

Results

Development of a murine model harboring an FGF23 conditional-null allele

To develop an *in vivo* model carrying conditional-null alleles for *Fgf23*, mouse exon 2 was targeted for Cre-mediated recombination (LoxP sites in introns 1 and 2; diagrammed in Figure 1A (upper panel)), as deletion of this exon is predicted to cause frame shift mutations after residue 70 and a stop codon after residue 89 in the predicted FGF23 protein (Supplemental Figure 1). The LoxP-*Fgf23* construct (see Methods) was delivered to ES cells, and standard protocols were used to derive mice chimeric for the floxed *Fgf23* allele. As determined by PCR and sequencing of founder line DNA, germline transmission of the flox-*Fgf23* allele ('flox' or 'f' allele; $Fgf23^{f/+}$ mice; Figure 1A (lower panel)) was confirmed. Following initial $Fgf23^{f/+}$ intercrosses, it was determined that the mice carrying homozygous, non-recombined LoxP-*Fgf23* alleles ($Fgf23^{f/f}$) were normal for serum phosphate, calcium, alkaline phosphatase, and intact and *C*-terminal FGF23 concentrations from 5–19 weeks of age when compared to $Fgf23^{f/+}$ and WT ($Fgf23^{+/+}$) littermates (see complete listing of biochemistries: Supplemental Table 1).

To test Cre-mediated recombination of the flox-*Fgf23* allele, $Fgf23^{f/+}$ mice were mated with widely-expressed *eIIa*-Cre transgenic mice by standard breeding regimen. Using PCR primers that spanned the floxed exon 2 region (Figure 1A), a 743 bp PCR product was amplified from genomic DNA of these mice (the 'Δ' allele; Figure 1B). When sequenced, this product showed the expected deletion of exon 2 with the junction of introns 1 and 3 with a single intervening LoxP site (Supplemental Figure 3). These results demonstrated that the LoxP sites within introns 1 and 2 flanking *Fgf23* exon 2 were correctly targeted and did not alter baseline FGF23 expression and phosphate metabolism.

Testing the functional LoxP-Fgf23 allele in vivo

To determine whether the Δ allele was null for FGF23 expression, the $Fgf23^{\Delta/+}$ mice were either intercrossed, or $Fgf23^{f/f}$ mice were bred with $Fgf23^{\Delta/+}$/*ella*-cre^{+} mice. Offspring with fully recombined *Fgf23* ($Fgf23^{\Delta/f}$/*ella*-cre^{+}; i.e. genotyped as harboring no remnant intact floxed-*Fgf23* alleles following exposure to Cre, approximately 40% of offspring) were much smaller than control littermates (Figure 1C). Biochemical analyses revealed that these $Fgf23^{\Delta/f}$/*ella*-cre^{+} mice had undetectable serum intact FGF23 ($p<0.01$; Figure 1D), which paralleled the lack of measureable serum intact FGF23 in $Fgf23^{\Delta/\Delta}$ mice (not shown). Similar to the reported *Fgf23*-KO mice, the $Fgf23^{\Delta/f}$/*ella*-cre^{+} mice were hyperphosphatemic compared to controls ($p<0.05$; Figure 1D) ([28], [29]), and had modestly, but not significantly reduced serum calcium. These mice also had elevated kidney vitamin D 1α-hydroxylase mRNA (*Cyp27a1*, $p<0.05$; Figure 1D), consistent with the loss of FGF23-mediated suppression of this gene. Intercrossed $Fgf23^{\Delta/\Delta}$ mice had undetectable serum intact FGF23

and undetectable femur Fgf23 mRNA (Supplemental Figure 4). Thus, targeted deletion of *Fgf23* exon 2 produced a conditional allele null for FGF23 expression.

Bone-specific FGF23 deletion and phosphate challenge

To test the contribution and localization of phosphate-sensitive FGF23 production, *Fgf23*$^{\Delta/f}$ mice (heterozygous Δ mice were used to potentially reduce the background of FGF23-expressing alleles) were bred to the Type Ia1 collagen 2.3kb promoter-cre transgenic line (Col2.3-cre, known to target early osteoblasts through to osteocytes. At 8 weeks of age, *Fgf23*$^{\Delta/f}$/Col2.3-cre^{+} mice maintained on control diet had serum intact FGF23 ~50% of same genotype *Fgf23*$^{\Delta/f}$/Col2.3-cre^{-} littermates (p<0.01; Figure 2A) which corresponded with a 75% reduction in femur Fgf23 mRNA (Figure 2A, *inset*). Additional phenotypes emerged when mice were placed on a two-week high phosphate ('HighP') diet at six weeks of age to induce FGF23 production (diet previously reported ([8])). After receiving the HighP diet, the *Fgf23*$^{\Delta/f}$/Col2.3-cre^{-} mice increased serum intact FGF23 2.1 fold (p<0.01 versus control diet; Figure 2A). In contrast, the *Fgf23*$^{\Delta/f}$/Col2.3-cre^{+} mice only slightly elevated intact FGF23, with serum concentrations significantly reduced compared to *Fgf23*$^{\Delta/f}$/Col2.3-cre^{-} mice receiving control or HighP diets (p<0.01; Figure 2A), consistent with an inability to produce FGF23 in response to changes in serum phosphate.

Next, to target FGF23 in osteocytes, the late osteoblast/osteocyte 8kb-promoter Dentin matrix protein-1-cre (Dmp1-cre) transgenic line was bred onto the flox-*Fgf23* background. Similar to the crosses with Col2.3-cre, *Fgf23*$^{\Delta/f}$/Dmp1-cre^{+} mice had a 40% reduction of basal intact FGF23 on control diet versus *Fgf23*$^{\Delta/f}$/Dmp1-cre^{-} controls (p<0.01; Figure 2B) and consistent with osteocytes maintaining basal FGF23 expression. Femur *Fgf23* mRNA was reduced, but did not reach statistical significance (Figure 2B, *inset*). With the provision of the HighP diet, *Fgf23*$^{\Delta/f}$/Dmp1-cre^{-} mice showed a significant increase in intact FGF23 (p<0.01; Figure 2B) whereas the *Fgf23*$^{\Delta/f}$/Dmp1-cre^{+} mice had a positive, but markedly blunted response (37% increased versus *Fgf23*$^{\Delta/f}$/Dmp1-cre^{-} mice, p<0.001; Figure 2B). Although differences in Cre efficiencies cannot be ruled out at this time, the increase in serum FGF23 following Dmp1-cre exposure and HighP diet was greater than the induction in *Fgf23*$^{\Delta/f}$/Col2.3-cre^{+} mice (p<0.01; Figure 2B).

Coincident with reduced FGF23 during phosphate challenge, the *Fgf23*$^{\Delta/f}$/Col2.3-cre^{+} mice had elevated serum phosphate concentrations versus *Fgf23*$^{\Delta/f}$/Col2.3-cre^{-} mice (p<0.01; Figure 2C), and versus same genotype, control diet littermates (p<0.01; Figure 2C). Serum phosphate was not different between *Fgf23*$^{\Delta/f}$/Dmp1-cre^{-} and *Fgf23*$^{\Delta/f}$/Dmp1-cre^{+} mice during control diet consumption, but after HighP diet, there was a significant elevation in both genotypes (p<0.05; Figure 2C), with a further elevation in the *Fgf23*$^{\Delta/f}$/Dmp1-cre^{+} mice (p<0.05; Figure 2C). Serum calcium levels were not different between genotype or dietary challenge (Figure 2D), and alkaline phosphatase was slightly reduced in *Fgf23*$^{\Delta/f}$/Col2.3-cre^{+} mice receiving HighP diet (p<0.05; Figure 2E). Serum PTH levels also responded to the HighP diet, as both the *Fgf23*$^{\Delta/f}$/Col2.3-cre^{-} and *Fgf23*$^{\Delta/f}$/Dmp1-cre^{-} mice showed a significant increase compared to those receiving control diet (p<0.05; Figure 2F). In contrast, PTH was not significantly increased in the *Fgf23*$^{\Delta/f}$/Col2.3-cre^{+} or *Fgf23*$^{\Delta/f}$/Dmp1-cre^{+} mice receiving the HighP diet (Figure 2F). No calcifications were observed in

the osteoblast/osteocyte targeted conditional mice. The *Fgf23*$^{\Delta/f}$/Col2.3-cre$^{+/-}$ and *Fgf23*$^{\Delta/f}$/Dmp1-cre$^{+/-}$ mice were also fed a high phosphate and low calcium diet reported to increase FGF23 ([37]); this diet produced similar results as the HighP diet for serum intact FGF23 (Supplemental Figure 5). Thus, when FGF23 was targeted in both osteoblasts and osteocytes using the Col2.3-cre, there was only a slight increase but when deleted from a more mature cell population with the Dmp1-cre, FGF23 showed a modest increase. These findings support that both osteoblasts and osteocytes contribute to basal and phosphate-sensitive serum FGF23 concentrations.

Rescue of the Hyp phenotype with bone-specific Fgf23 targeting

The metabolic bone disorder XLH is due to loss of function mutations in the *Phosphate regulating gene with homology to endopeptidases* (*PHEX*)([1, 38]). The murine XLH model *Hyp* has a large 3′ *Phex* deletion and reflects the majority of the XLH patient disease phenotypes including elevated FGF23, small size, hypophosphatemia with inappropriately normal 1,25D, and rickets/osteomalacia ([39, 40]). It was previously demonstrated that when *Hyp* and global *Fgf23*-KO mice were crossed, the offspring produced were not grossly and biochemically different from the *Fgf23*-KO mice ([28, 29]), as the *Hyp*/*Fgf23*-KO mice were small, hyperphosphatemic, had skeletal and ectopic calcifications, and undetectable serum FGF23 ([28, 29]). Although the role of *PHEX* in phosphate handling remains unclear, its loss of function mutations were previously shown to result in excess FGF23 produced during an osteoblast/osteocyte differentiation defect, therefore *Fgf23* was targeted on the *Hyp* background using the osteoblast Col2.3-cre. In contrast to *Hyp*/*Fgf23*$^{\Delta/+}$/Col2.3-cre$^{+/-}$ (‘*Hyp*’) mice, *Hyp*/*Fgf23*$^{\Delta/f}$/Col2.3-cre^{+} mice resembled *Fgf23*$^{\Delta/+}$/Col2.3-cre^{+} (phenotypically normal) mice and were normalized for body size (Figure 3A), as well as femur (Figure 3B) and tail length (Figure 3B). At baseline (4 weeks of age) circulating intact FGF23 in *Hyp*/*Fgf23*$^{\Delta/f}$/Col2.3-cre^{+} mice was ~40% of *Fgf23*$^{\Delta/+}$/Col2.3-cre^{+} ($p<0.01$) and <4% of *Hyp* concentrations ($p<0.01$; Figure 3C), and did not vary over the time course (up to 8 weeks of age) as assessed by interim bleeds (Figure 3C). The *Hyp* mouse is known to manifest reduced serum phosphate and elevated PTH, which was confirmed (Figure 3D). Consistent with reversal of the *Hyp* disease phenotypes, serum phosphate and PTH in *Hyp*/*Fgf23*$^{\Delta/f}$/Col2.3-cre^{+} mice was normal versus *Hyp* mice ($p<0.01$ and $p<0.05$, respectively; Figure 3D) and not different from *Fgf23*$^{\Delta/+}$/Col2.3-cre^{+} mice (Figure 3D). Thus, in contrast to complete ablation of *Fgf23*, reduction of serum FGF23 to below WT baseline levels can rescue *Hyp* disease phenotypes without the severe manifestations of hyperphosphatemia.

The *Hyp* skeletal phenotype is characterized by osteomalacia, abnormal growth plate, as well as widened distal metaphyses due to the prevailing hypophosphatemia and inhibited mineralization. As observed by μCT, compared to femurs from *Fgf23*$^{\Delta/+}$/Col2.3-cre^{+} mice, femurs from *Hyp*/*Fgf23*$^{\Delta/f}$/Col2.3-cre^{+} mice displayed almost normal shape, lacking the widened distal metaphysis and growth plate typically observed in *Hyp* mice ([1, 39]), while also exhibiting higher trabecular bone volume (Figure 4A). Indeed, the metaphyses of *Hyp*/*Fgf23*$^{\Delta/f}$/Col2.3-cre^{+} femurs lacked marrow space or trabeculae definition due to the abundant bone, and had markedly increased metaphyseal trabecular BV/TV, compared to *Hyp* and *Fgf23*$^{\Delta/+}$/Col2.3-cre^{+} (Table 1). This osteopetrotic phenotype was not found by μCT in *Fgf23*$^{\Delta/f}$/Col2.3-cre^{+} mice (not shown). In cortical bone, *Hyp*/*Fgf23*$^{\Delta/f}$/Col2.3-cre^{+}

cortical thickness and bone area/tissue area (BA/TA) were normalized versus *Hyp* femurs to levels similar to *Fgf23*$^{\Delta/+}$/Col2.3-cre^{+} (Table 1). Cortical porosity was also high in *Hyp* femurs (Table 1). Von Kossa staining showed a dramatic correction of the osteomalacia in *Hyp*/*Fgf23*$^{\Delta/f}$/Col2.3-cre^{+}, in concert with increased mineralized bone (Figure 4C), consistent with the μCT scans. Qualitative evaluation of the growth plate revealed almost complete rescue with prototypical alignment of proliferative chondrocytes and hypertrophic/apoptotic chondrocytes in the *Hyp*/*Fgf23*$^{\Delta/f}$/Col2.3-cre^{+}. There was also clear ossification of cartilage in the lower portions of the plate. Dynamic histomorphometry analyses showed distinct separation of labels in *Hyp*/*Fgf23*$^{\Delta/f}$/Col2.3-cre^{+} femurs, similar to *Fgf23*$^{\Delta/+}$/Col2.3-cre^{+} mice, whereas *Hyp* displayed very poor label uptake and virtually no separation, in accord with its well-characterized mineralization impairment (Figure 4D). Mineral apposition rate, mineralizing surface, and bone formation rate/bone surface were similar between *Hyp*/*Fgf23*$^{\Delta/f}$/Col2.3-cre^{+} and *Fgf23*$^{\Delta/+}$/Col2.3-cre^{+} for both the periosteal and endocortical surfaces (Table 1). Therefore, targeted reduction of FGF23 in *Hyp* restores bone length but cannot overcome the intrinsic *Hyp* osteoblastic defects to fully normalize general architecture.

In summary, when *Fgf23* is targeted in the early osteoblast and in osteocytes, the recombined *Fgf23* allele produces an animal with serum concentrations significantly reduced in the basal state, supporting that osteoblasts and osteocytes contribute to normal circulating FGF23 concentrations. Dietary phosphate challenge demonstrated the ability of these cells to respond to increased serum phosphorus by inducing FGF23. Ultimately, inability of FGF23 to fully respond to this challenge in the conditional deletion models resulted in hyperphosphatemia. Finally, recombination of the *Fgf23* allele in early osteoblasts demonstrated that over-riding the *Hyp* defect of inappropriate and elevated FGF23 production during hypophosphatemia by restricting serum FGF23 to below WT levels rescued the majority of disease manifestations.

Discussion

The use of genetic mouse models that delete or over express critical components of the FGF23 bone-kidney signaling axis have markedly enhanced the understanding of phosphate metabolism. Global *Fgf23* knockout mice are phenotypically similar to wild type (WT) littermates at birth ([28–30]). These mice then become severely hyperphosphatemic with elevated serum calcium and 1,25D over the next several weeks ([28–30]). FGF23 interacts with an FGF receptor (FGFR) and αKL in the kidney to elicit a renal phosphaturic response ([3, 4]). Consistent with FGF23-αKL interactions, homozygous deletion of murine α*Kl* results in an animal exhibiting a phenotype virtually identical to the *Fgf23-KO* mice, with hyperphosphatemia, elevated 1,25D, and reduced PTH ([4]). The primary endocrine difference between *Fgf23*-null and α*Kl*-null is that the latter have markedly elevated circulating FGF23 ([4]), likely as a compensatory response to end-organ resistance of the kidneys to FGF23 signaling, and a positive feedback loop resulting from the prevailing elevated 1,25D and hyperphosphatemia. Indeed, placing α*Kl*-null mice on a low phosphate diet ([41]) or mating the *Fgf23*-KO mouse to the *Vdr*-KO mouse ([42]) normalizes the overwhelming majority of the endocrine manifestations, establishing defective phosphate metabolism as the primary source of the disease phenotypes. Using the global *eIIa*-cre, we determined that the floxed-

Fgf23 allele could undergo homologous recombination. This Cre line is known to have mosaicism ([43], [44]), however a substantial portion of the flox-*Fgf23*/*eIIa*-cre offspring fully recapitulated the phenotype of the global *Fgf23*-KO mice. In comparison to the global *Fgf23*-null mice, while receiving a normal diet the *Fgf23* conditional-null mice crossed with the Col2.3- and Dmp1-cre transgenic lines had normal serum phosphate concentrations, PTH, calcium, and alkaline phosphatase. Importantly, intact serum FGF23 concentrations were approximately 50% of the respective Cre- controls. Upon challenge with high phosphate diet, the Cre^+ mice could not maintain normal phosphate metabolism, and similar to the global *Fgf23*-KO had elevated serum phosphate with normocalcemia. PTH was similarly elevated in the flox-*Fgf23*/Col2.3-cre^- and flox-*Fgf23*/Dmp1-cre^- mice receiving HighP diet, however this effect was blunted in the flox-*Fgf23*/Col2.3-cre^+ and flox-*Fgf23*/Dmp1-cre^+ mice. Whether this response was to due to direct or indirect effects of the inability to fully increase FGF23 in response to high phosphate diet remains to be determined. The localization of the cell populations that increase FGF23 in response to elevated serum phosphate in these models (and patients) are unclear however, as to date no 'stand-alone' phosphate sensing receptor analogous to the calcium-sensing receptor (CASR) has been identified. Herein, it was demonstrated that targeted deletion of FGF23 from both osteoblasts and osteocytes restricted the ability of mice to normalize serum phosphate following challenge with high phosphate diet. Indeed, when comparing floxed-*Fgf23* mice that were bred onto the Col2.3-cre or the Dmp1-cre backgrounds, both groups had reduced basal intact FGF23 concentrations. When challenged with high phosphate diet, the Col2.3-cre^+ mice could not significantly elevate FGF23 above their reduced basal levels, whereas the Dmp1-cre^+ mice had the ability to partially compensate, and raised FGF23 approximately 35–40% of Dmp1-cre^- mice. FGF23 production in osteocytes is critical to disease models such as the *Dmp1*-KO mouse (modeling ARHR type 1) ([16]), the deletion of FGF23 from both early osteoblasts and late osteoblast/osteocytes compromises the ability to respond to phosphate challenge, thus osteoblasts and osteocytes play a significant role in phosphate-mediated FGF23 production. Additionally, the mechanisms responsible for the biological 'set point' for circulating FGF23 and serum phosphate are unknown. It has been shown that normal individuals' serum FGF23 levels vary quite widely but that serum phosphate is maintained within a fairly narrow range ([20], [45], [46]). We found that selective FGF23 deletion in osteoblasts or osteocytes similarly reduced baseline concentrations yet did not elicit a global knockout phenotype, therefore multiple cell types may be responsible for maintenance of normal circulating intact FGF23.

Mouse models involving pathways that post-translationally modify FGF23 have also been important for relating patient phenotypes to molecular disease mechanisms. Animals null for the *O*-glycosylating enzyme GalNAc-T3 (*Galnt3*) cannot glycosylate FGF23 on threonine (T) 178 within the FGF23 proprotein convertase $R_{176}HT_{178}R_{179}$/SAE motif, and thus produce FGF23 that is rapidly cleaved by the intracellular protease furin ([25]). These mice produce intact FGF23 at concentrations approximately 50% of WT, similar to our results for the $Fgf23^{\Delta/f}$/Col2.3-cre and $Fgf23^{\Delta/f}$/Dmp1-cre mice at baseline. Provision of a high phosphate diet to *Galnt3*-KO mice results in tumoral calcinosis phenotype ([47]), reflective of some patients with loss of function mutations in *GALNT3* ([23], [48], [49]). We found that with phosphate challenge both *Fgf23*/Col2.3-cre and *Fgf23*/Dmp1-cre conditional-nulls retained

the capacity to produce some intact FGF23, at approximately one-half of the basal level of WT mice. With exposure to bone specific Cre expression, these mice were also hyperphosphatemic upon high phosphate dietary challenge. This expression profile is reflective of patients with hfTC *GALNT3* and *FGF23* missense mutations ([21], [22], [50]), where the ability to produce FGF23 at minimal levels and carry out low-level renal phosphate metabolism likely prevents early death, as reported in complete *Fgf23*-null mice ([28], [29]) or a severe hfTC phenotype as reported in a family with an *FGF23* deletion and missense mutation ([51]). Serum FGF23 was detectable after targeting recombination to osteoblasts and osteocytes, therefore it is possible that FGF23 is also produced in other cell types within bone such as chondrocytes ([52]), or extra-skeletal tissues such as skin and brain ([53]), as well as heart ([54]). Additionally, it cannot be ruled out at this time that some inefficiency of the respective Cre transgenic lines accounts in part for the detectable serum FGF23. The contributions of these other potential sites to circulating FGF23 at baseline and during phosphate diet challenge is currently unknown. Therefore, future studies targeting cells outside of osteoblasts and osteocytes will be important for understanding FGF23 bioactivity under normal circumstances and during disease modeling.

The knockout models involving FGF23 and its co-receptor αKL have been used in breeding strategies to genetically determine the mechanisms underlying diseases of FGF23 over production. When the global *Fgf23*-KO was crossed with the mouse model of XLH, the *Hyp* mouse, the *Fgf23*-KO phenotype dominated the *Hyp* phenotype causing severe hyperphosphatemia. ([28], [29]). The *Hyp* mouse has a defect in osteoblast differentiation, producing cortical bone cells with elevated Type 1 collagen, matrix protein disturbances ([40]), as well as increased alkaline phosphatase and FGF23 ([7], [55], [56]). Additionally, this model has an intrinsic defect whereby FGF23 is approximately 10-fold elevated in the face of significant hypophosphatemia ([57]), typically a potent FGF23 suppressor via negative feedback. We found that when *Fgf23* was targeted in the *Hyp*/*Fgf23*$^{\Delta/f}$/Col2.3-cre cross, the mice had relatively normal body size, but markedly elevated bone volume as well as normal femur length and shape, as opposed to the *Hyp* manifestations of stunted growth and widened metaphyses due to the severe hypophosphatemia ([39]). Our findings demonstrated that deleting *Fgf23* from osteoblasts/osteocytes in *Hyp* ablates the manifestations of the inappropriately elevated FGF23, as well as supported the concept that providing even a minor amount of FGF23-dependent phosphate metabolism allows the skeleton to more appropriately develop. However, the *Hyp*/XLH intrinsic cellular defect in the context of slight hyperphosphatemia due to loss of FGF23 resulted in over-mineralization of trabecular bone in *Hyp*/*Fgf23*$^{\Delta/f}$/Col2.3-cre^{+} mice. In the reported global *Hyp*/*Fgf23*-KO mice, bone length and BMD were not restored to WT values, but this cross did show an area of intense mineralization proximal to the growth plate ([29]), similar to the *Hyp*/*Fgf23*$^{\Delta/f}$/Col2.3-cre^{+} mice. In the *Hyp*/*αKl*-KO cross, bone length also remained shortened and thus similar to *αKl*-KO mice and far shorter than in WT. However, *Hyp*/*αKl*-KO mice had significantly increased trabecular bone density with levels above those of WT controls ([58]). The *Hyp*/*Fgf23*$^{\Delta/f}$/Col2.3-cre cross resulted in notable rescue of bone length and normalization of bone shape versus *Hyp* mice. It is unclear why rescue of specific portions of the skeletal phenotype, such as shape, occurs when FGF23 bioactivity is absent during global deletion of *Fgf23* ([28]), but bone length is not. Although not directly tested herein, with similarly

reduced baseline serum FGF23 concentrations between the flox-*Fgf23*/Col2.3-cre and flox-*Fgf23*/Dmp1-cre mice, taken together with early expression of Dmp1 in *Hyp* osteoblasts/osteocytes ([59]), it is anticipated that a *Hyp*/flox-*Fgf23*/Dmp1-cre cross could produce a similar rescue. A circulating form of αKL ('cKL') may interact with osteoblasts ([60]), but whether blood αKL affects bone development in the *Fgf23*-null environment is currently unknown.

Novel therapies that involve inhibiting FGF23 activity with neutralizing antibodies are currently in clinical trials for XLH ([61], [62]), and were previously shown to correct the major manifestations of hypophosphatemic rickets in the *Hyp* mouse ([63]). The *Hyp*/*Fgf23*$^{\Delta/f}$/Col2.3-Cre cross resulted in significant reductions in circulating FGF23 compared to *Hyp* and WT mice, and rescued the hypophosphatemia and *Hyp* skeletal disease phenotypes with almost complete restoration of normal bone length and shape. These findings support that the inhibition of bioactive FGF23 production to at least one-half of control serum concentrations (or <4% of *Hyp*) can restore almost normal phosphate metabolism associated with uncontrollable FGF23 excess. Converse to loss of function mutations in *FGF23*, *αKL*, and *GALNT3*, FGF23 transgenic mice whether under control of the Type 1 collagen promoter (*Col1a1*) ([6]) or β-actin ([27]), have severe hypophosphatemia with little to no change in serum calcium, low 1,25D levels and reduced bone mineral density (BMD) ([6], [27]). A murine model of the ADHR syndrome carrying an R176Q-*Fgf23* point mutation can be induced to express elevated FGF23 and an ADHR phenotype during iron deficiency anemia ([12], [64]). Additionally, although genetically distinct, global or bone-specific conditional knockout of *Dmp1* (human *DMP1* mutations cause autosomal recessive hypophosphatemic rickets (ARHR) Type 1) ([16]), and the kinase Family with sequence similarity 20, member C (*FAM20C*; mutations cause ARHR Type 3 or 'Raine syndrome') ([65]) result in animals that over express FGF23 and manifest a hypophosphatemic rickets phenotype similar to *Hyp* mice. Consistent with its proposed role as a key mediator of renal phosphate handling, mice with a common denominator of high circulating FGF23 reproduce the majority of the biochemical and skeletal defects of patients with ADHR, ARHR, XLH and TIO. Thus, our results support the idea that control of FGF23 bioactivity through a targeted, conditional approach could also be useful for dissecting heterogeneous disease mechanisms as well as for testing specific therapeutic approaches in diverse models of FGF23 over production through FGF23 reduction in specific cell populations.

In summary, an animal with a conditional *Fgf23* allele was developed, and demonstrated that osteoblasts and osteocytes contribute to the maintenance of normal circulating FGF23 levels. Finally, restricting osteoblasts/osteocytes from inappropriately over-producing FGF23 during prevailing hypophosphatemia can rescue severe *Hyp* phenotypes.

Supplementary Material

Refer to Web version on PubMed Central for supplementary material.

Acknowledgments

The authors would like to acknowledge NIH grants R21-AR059278, R01-DK063934 and R01-DK95784 (KEW); F32-AR065389 (ELC); T32-HL007910 and an American Heart Association Postdoctoral Fellowship

16POST-27260108 (JMH); R01-AR062002 (MRA); R01-AR059357 and VA-BX002104 (TB); the Indiana Genomics Initiative (INGEN), supported in part by the Lilly Endowment, Inc.; The David Weaver Professorship and a Showalter Scholar award through the Ralph W. and Grace M. Showalter Research Trust (KEW). The authors also thank Jeff Lavigne from Immutopics, Int'l. for initial provision of rodent intact FGF23 ELISAs, Dr. Alex Robling for assistance with the radiographs, and Anthony Acton for assistance with biochemical analyses.

Bibliography

1. Tenenhouse, HS.; Econs, MJ. The Metabolic and Molecular Bases of Inherited Disease;. Valle, D., editor. New York: The McGraw-Hill Companies; 2001. p. 1-9.
2. White KE, Larsson TE, Econs MJ. The roles of specific genes implicated as circulating factors involved in normal and disordered phosphate homeostasis: frizzled related protein-4, matrix extracellular phosphoglycoprotein, and fibroblast growth factor 23. Endocr Rev. 2006; 27(3):221–41. [PubMed: 16467171]
3. Kurosu H, Ogawa Y, Miyoshi M, Yamamoto M, Nandi A, Rosenblatt KP, Baum MG, Schiavi S, Hu MC, Moe OW, et al. Regulation of fibroblast growth factor-23 signaling by klotho. J Biol Chem. 2006; 281(10):6120–3. [PubMed: 16436388]
4. Urakawa I, Yamazaki Y, Shimada T, Iijima K, Hasegawa H, Okawa K, Fujita T, Fukumoto S, Yamashita T. Klotho converts canonical FGF receptor into a specific receptor for FGF23. Nature. 2006; 444(7120):770–4. [PubMed: 17086194]
5. Shimada T, Mizutani S, Muto T, Yoneya T, Hino R, Takeda S, Takeuchi Y, Fujita T, Fukumoto S, Yamashita T. Cloning and characterization of FGF23 as a causative factor of tumor-induced osteomalacia. Proc Natl Acad Sci USA. 2001; 98(11):6500–5. [PubMed: 11344269]
6. Larsson T, Marsell R, Schipani E, Ohlsson C, Ljunggren O, Tenenhouse HS, Juppner H, Jonsson KB. Transgenic mice expressing fibroblast growth factor 23 under the control of the alpha1(I) collagen promoter exhibit growth retardation, osteomalacia, and disturbed phosphate homeostasis. Endocrinology. 2004; 145(7):3087–94. [PubMed: 14988389]
7. Liu S, Guo R, Simpson LG, Xiao ZS, Burnham CE, Quarles LD. Regulation of fibroblastic growth factor 23 expression but not degradation by PHEX. J Biol Chem. 2003; 278(39):37419–26. [PubMed: 12874285]
8. Perwad F, Azam N, Zhang MY, Yamashita T, Tenenhouse HS, Portale AA. Dietary and serum phosphorus regulate fibroblast growth factor 23 expression and 1,25-dihydroxyvitamin D metabolism in mice. Endocrinology. 2005; 146(12):5358–64. [PubMed: 16123154]
9. Liu S, Tang W, Zhou J, Stubbs JR, Luo Q, Pi M, Quarles LD. Fibroblast growth factor 23 is a counter-regulatory phosphaturic hormone for vitamin D. J Am Soc Nephrol. 2006; 17(5):1305–15. [PubMed: 16597685]
10. Shimada T, Hasegawa H, Yamazaki Y, Muto T, Hino R, Takeuchi Y, Fujita T, Nakahara K, Fukumoto S, Yamashita T. FGF-23 is a potent regulator of vitamin D metabolism and phosphate homeostasis. J Bone Miner Res. 2004; 19(3):429–35. [PubMed: 15040831]
11. Rhee Y, Bivi N, Farrow E, Lezcano V, Plotkin LI, White KE, Bellido T. Parathyroid hormone receptor signaling in osteocytes increases the expression of fibroblast growth factor-23 in vitro and in vivo. Bone. 2011; 49(4):636–43. [PubMed: 21726676]
12. Farrow EG, Yu X, Summers LJ, Davis SI, Fleet JC, Allen MR, Robling AG, Stayrook KR, Jideonwo V, Magers MJ, et al. Iron deficiency drives an autosomal dominant hypophosphatemic rickets (ADHR) phenotype in fibroblast growth factor-23 (Fgf23) knock-in mice. Proc Natl Acad Sci U S A. 2011; 108(46):E1146–55. [PubMed: 22006328]
13. Xiao L, Esliger A, Hurley MM. Nuclear fibroblast growth factor 2 (FGF2) isoforms inhibit bone marrow stromal cell mineralization through FGF23/FGFR/MAPK in vitro. J Bone Miner Res. 2013; 28(1):35–45. [PubMed: 22836867]
14. Xiao Z, Huang J, Cao L, Liang Y, Han X, Quarles LD. Osteocyte-specific deletion of Fgfr1 suppresses FGF23. PLoS One. 2014; 9(8):e104154. [PubMed: 25089825]
15. ADHR-Consortium. Autosomal dominant hypophosphataemic rickets is associated with mutations in FGF23. Nature genetics. 2000; 26(3):345–8. [PubMed: 11062477]

16. Feng JQ, Ward LM, Liu S, Lu Y, Xie Y, Yuan B, Yu X, Rauch F, Davis SI, Zhang S, et al. Loss of DMP1 causes rickets and osteomalacia and identifies a role for osteocytes in mineral metabolism. Nature genetics. 2006; 38(11):1310–5. [PubMed: 17033621]
17. Lorenz-Depiereux B, Bastepe M, Benet-Pages A, Amyere M, Wagenstaller J, Muller-Barth U, Badenhoop K, Kaiser SM, Rittmaster RS, Shlossberg AH, et al. DMP1 mutations in autosomal recessive hypophosphatemia implicate a bone matrix protein in the regulation of phosphate homeostasis. Nature genetics. 2006; 38(11):1248–50. [PubMed: 17033625]
18. Lorenz-Depiereux B, Schnabel D, Tiosano D, Hausler G, Strom TM. Loss-of-function ENPP1 mutations cause both generalized arterial calcification of infancy and autosomal-recessive hypophosphatemic rickets. Am J Hum Genet. 2010; 86(2):267–72. [PubMed: 20137773]
19. Ababneh FK, AlSwaid A, Youssef T, Al Azzawi M, Crosby A, AlBalwi MA. Hereditary deletion of the entire FAM20C gene in a patient with Raine syndrome. Am J Med Genet A. 2013; 161A(12):3155–60. [PubMed: 24039075]
20. Jonsson KB, Zahradnik R, Larsson T, White KE, Sugimoto T, Imanishi Y, Yamamoto T, Hampson G, Koshiyama H, Ljunggren O, et al. Fibroblast growth factor 23 in oncogenic osteomalacia and X-linked hypophosphatemia. N Engl J Med. 2003; 348(17):1656–63. [PubMed: 12711740]
21. Larsson T, Yu X, Davis SI, Draman MS, Mooney SD, Cullen MJ, White KE. A novel recessive mutation in fibroblast growth factor-23 causes familial tumoral calcinosis. J Clin Endocrinol Metab. 2005; 90(4):2424–7. [PubMed: 15687325]
22. Benet-Pages A, Orlik P, Strom TM, Lorenz-Depiereux B. An FGF23 missense mutation causes familial tumoral calcinosis with hyperphosphatemia. Hum Mol Genet. 2005; 14(3):385–90. [PubMed: 15590700]
23. Topaz O, Shurman DL, Bergman R, Indelman M, Ratajczak P, Mizrachi M, Khamaysi Z, Behar D, Petronius D, Friedman V, et al. Mutations in GALNT3, encoding a protein involved in O-linked glycosylation, cause familial tumoral calcinosis. Nature genetics. 2004; 36(6):579–81. [PubMed: 15133511]
24. Ichikawa S, Imel EA, Kreiter ML, Yu X, Mackenzie DS, Sorenson AH, Goetz R, Mohammadi M, White KE, Econs MJ. A homozygous missense mutation in human KLOTHO causes severe tumoral calcinosis. J Clin Invest. 2007; 117(9):2684–91. [PubMed: 17710231]
25. Ichikawa S, Sorenson AH, Austin AM, Mackenzie DS, Fritz TA, Moh A, Hui SL, Econs MJ. Ablation of the Galnt3 gene leads to low-circulating intact fibroblast growth factor 23 (Fgf23) concentrations and hyperphosphatemia despite increased Fgf23 expression. Endocrinology. 2009; 150(6):2543–50. [PubMed: 19213845]
26. Bergwitz C, Banerjee S, Abu-Zahra H, Kaji H, Miyauchi A, Sugimoto T, Juppner H. Defective O-glycosylation due to a novel homozygous S129P mutation is associated with lack of fibroblast growth factor 23 secretion and tumoral calcinosis. J Clin Endocrinol Metab. 2009; 94(11):4267–74. [PubMed: 19837926]
27. Shimada T, Urakawa I, Yamazaki Y, Hasegawa H, Hino R, Yoneya T, Takeuchi Y, Fujita T, Fukumoto S, Yamashita T. FGF-23 transgenic mice demonstrate hypophosphatemic rickets with reduced expression of sodium phosphate cotransporter type IIa. Biochem Biophys Res Commun. 2004; 314(2):409–14. [PubMed: 14733920]
28. Sitara D, Razzaque MS, Hesse M, Yoganathan S, Taguchi T, Erben RG, Juppner H, Lanske B. Homozygous ablation of fibroblast growth factor-23 results in hyperphosphatemia and impaired skeletogenesis, and reverses hypophosphatemia in Phex-deficient mice. Matrix biology : journal of the International Society for Matrix Biology. 2004; 23(7):421–32. [PubMed: 15579309]
29. Liu S, Zhou J, Tang W, Jiang X, Rowe DW, Quarles LD. Pathogenic role of Fgf23 in Hyp mice. Am J Physiol Endocrinol Metab. 2006; 291(1):E38–49. [PubMed: 16449303]
30. Shimada T, Kakitani M, Yamazaki Y, Hasegawa H, Takeuchi Y, Fujita T, Fukumoto S, Tomizuka K, Yamashita T. Targeted ablation of Fgf23 demonstrates an essential physiological role of FGF23 in phosphate and vitamin D metabolism. J Clin Invest. 2004; 113(4):561–8. [PubMed: 14966565]
31. Liu F, Woitge HW, Braut A, Kronenberg MS, Lichtler AC, Mina M, Kream BE. Expression and activity of osteoblast-targeted Cre recombinase transgenes in murine skeletal tissues. The International journal of developmental biology. 2004; 48(7):645–53. [PubMed: 15470637]

32. Yang W, Lu Y, Kalajzic I, Guo D, Harris MA, Gluhak-Heinrich J, Kotha S, Bonewald LF, Feng JQ, Rowe DW, et al. Dentin matrix protein 1 gene cis-regulation: use in osteocytes to characterize local responses to mechanical loading in vitro and in vivo. J Biol Chem. 2005; 280(21):20680–90. [PubMed: 15728181]
33. Lorenz-Depiereux B, Guido VE, Johnson KR, Zheng QY, Gagnon LH, Bauschatz JD, Davisson MT, Washburn LL, Donahue LR, Strom TM, et al. New intragenic deletions in the Phex gene clarify X-linked hypophosphatemia-related abnormalities in mice. Mamm Genome. 2004; 15(3): 151–61. [PubMed: 15029877]
34. Bouxsein ML, Boyd SK, Christiansen BA, Guldberg RE, Jepsen KJ, Muller R. Guidelines for assessment of bone microstructure in rodents using micro-computed tomography. J Bone Miner Res. 2010; 25(7):1468–86. [PubMed: 20533309]
35. Parfitt AM, Drezner MK, Glorieux FH, Kanis JA, Malluche H, Meunier PJ, Ott SM, Recker RR. Bone histomorphometry: standardization of nomenclature, symbols, and units. Report of the ASBMR Histomorphometry Nomenclature Committee. J Bone Miner Res. 1987; 2(6):595–610. [PubMed: 3455637]
36. Livak KJ, Schmittgen TD. Analysis of relative gene expression data using real-time quantitative PCR and the 2(−Delta Delta C(T)) Method. Methods. 2001; 25(4):402–8. [PubMed: 11846609]
37. Sabbagh Y, Graciolli FG, O'Brien S, Tang W, dos Reis LM, Ryan S, Phillips L, Boulanger J, Song W, Bracken C, et al. Repression of osteocyte Wnt/beta-catenin signaling is an early event in the progression of renal osteodystrophy. J Bone Miner Res. 2012; 27(8):1757–72. [PubMed: 22492547]
38. HYP-Consortium. A gene (PEX) with homologies to endopeptidases is mutated in patients with X-linked hypophosphatemic rickets. The HYP Consortium. Nature genetics. 1995; 11(2):130–6. [PubMed: 7550339]
39. Beck L, Soumounou Y, Martel J, Krishnamurthy G, Gauthier C, Goodyer CG, Tenenhouse HS. Pex/PEX tissue distribution and evidence for a deletion in the 3′ region of the Pex gene in X-linked hypophosphatemic mice. J Clin Invest. 1997; 99(6):1200–9. [PubMed: 9077527]
40. Miao D, Bai X, Panda D, McKee M, Karaplis A, Goltzman D. Osteomalacia in hyp mice is associated with abnormal phex expression and with altered bone matrix protein expression and deposition. Endocrinology. 2001; 142(2):926–39. [PubMed: 11159866]
41. Segawa H, Yamanaka S, Ohno Y, Onitsuka A, Shiozawa K, Aranami F, Furutani J, Tomoe Y, Ito M, Kuwahata M, et al. Correlation between hyperphosphatemia and type II Na-Pi cotransporter activity in klotho mice. Am J Physiol Renal Physiol. 2007; 292(2):F769–79. [PubMed: 16985213]
42. Hesse M, Frohlich LF, Zeitz U, Lanske B, Erben RG. Ablation of vitamin D signaling rescues bone, mineral, and glucose homeostasis in Fgf-23 deficient mice. Matrix biology : journal of the International Society for Matrix Biology. 2007; 26(2):75–84. [PubMed: 17123805]
43. Lakso M, Pichel JG, Gorman JR, Sauer B, Okamoto Y, Lee E, Alt FW, Westphal H. Efficient in vivo manipulation of mouse genomic sequences at the zygote stage. Proc Natl Acad Sci U S A. 1996; 93(12):5860–5. [PubMed: 8650183]
44. Holzenberger M, Lenzner C, Leneuve P, Zaoui R, Hamard G, Vaulont S, Bouc YL. Cre-mediated germline mosaicism: a method allowing rapid generation of several alleles of a target gene. Nucleic acids research. 2000; 28(21):E92. [PubMed: 11058142]
45. Imel EA, Hui SL, Econs MJ. FGF23 concentrations vary with disease status in autosomal dominant hypophosphatemic rickets. J Bone Miner Res. 2007; 22(4):520–6. [PubMed: 17227222]
46. Yamazaki Y, Okazaki R, Shibata M, Hasegawa Y, Satoh K, Tajima T, Takeuchi Y, Fujita T, Nakahara K, Yamashita T, et al. Increased circulatory level of biologically active full-length FGF-23 in patients with hypophosphatemic rickets/osteomalacia. J Clin Endocrinol Metab. 2002; 87(11):4957–60. [PubMed: 12414858]
47. Ichikawa S, Gray AK, Padgett LR, Reilly AM, Unsicker TR. High dietary phosphate intake induces development of ectopic calcifications in a murine model of familial tumoral calcinosis. J Bone Miner Res. 2014; 29(9):2017–23. [PubMed: 24692172]
48. Frishberg Y, Topaz O, Bergman R, Behar D, Fisher D, Gordon D, Richard G, Sprecher E. Identification of a recurrent mutation in GALNT3 demonstrates that hyperostosis-

hyperphosphatemia syndrome and familial tumoral calcinosis are allelic disorders. J Mol Med. 2005; 83(1):33–8. [PubMed: 15599692]

49. Garringer HJ, Fisher C, Larsson TE, Davis SI, Koller DL, Cullen MJ, Draman MS, Conlon N, Jain A, Fedarko NS, et al. The role of mutant UDP-N-acetyl-alpha-D-galactosamine-polypeptide N-acetylgalactosaminyltransferase 3 in regulating serum intact fibroblast growth factor 23 and matrix extracellular phosphoglycoprotein in heritable tumoral calcinosis. J Clin Endocrinol Metab. 2006; 91(10):4037–42. [PubMed: 16868048]
50. Garringer HJ, Malekpour M, Esteghamat F, Mortazavi SM, Davis SI, Farrow EG, Yu X, Arking DE, Dietz HC, White KE. Molecular genetic and biochemical analyses of FGF23 mutations in familial tumoral calcinosis. Am J Physiol Endocrinol Metab. 2008; 295(4):E929–37. [PubMed: 18682534]
51. Shah A, Miller CJ, Nast CC, Adams MD, Truitt B, Tayek JA, Tong L, Mehtani P, Monteon F, Sedor JR, et al. Severe vascular calcification and tumoral calcinosis in a family with hyperphosphatemia: a fibroblast growth factor 23 mutation identified by exome sequencing. Nephrol Dial Transplant. 2014; 29(12):2235–43. [PubMed: 25378588]
52. Raimann A, Ertl DA, Helmreich M, Sagmeister S, Egerbacher M, Haeusler G. Fibroblast growth factor 23 and Klotho are present in the growth plate. Connective tissue research. 2013; 54(2):108–17. [PubMed: 23206185]
53. Yamashita T, Yoshioka M, Itoh N. Identification of a novel fibroblast growth factor, FGF-23, preferentially expressed in the ventrolateral thalamic nucleus of the brain. Biochem Biophys Res Commun. 2000; 277(2):494–8. [PubMed: 11032749]
54. Leifheit-Nestler M, Grosse Siemer R, Flasbart K, Richter B, Kirchhoff F, Ziegler WH, Klintschar M, Becker JU, Erbersdobler A, Aufricht C, et al. Induction of cardiac FGF23/FGFR4 expression is associated with left ventricular hypertrophy in patients with chronic kidney disease. Nephrol Dial Transplant. 2015
55. Liu S, Tang W, Zhou J, Vierthaler L, Quarles LD. Distinct roles for intrinsic osteocyte abnormalities and systemic factors in regulation of FGF23 and bone mineralization in Hyp mice. Am J Physiol Endocrinol Metab. 2007; 293(6):E1636–44. [PubMed: 17848631]
56. Farrow EG, Summers LJ, Schiavi SC, McCormick JA, Ellison DH, White KE. Altered renal FGF23-mediated activity involving MAPK and Wnt: effects of the Hyp mutation. J Endocrinol. 2010; 207(1):67–75. [PubMed: 20675303]
57. Ichikawa S, Austin AM, Gray AK, Econs MJ. A Phex mutation in a murine model of X-linked hypophosphatemia alters phosphate responsiveness of bone cells. J Bone Miner Res. 2012; 27(2): 453–60. [PubMed: 22006791]
58. Brownstein CA, Zhang J, Stillman A, Ellis B, Troiano N, Adams DJ, Gundberg CM, Lifton RP, Carpenter TO. Increased bone volume and correction of HYP mouse hypophosphatemia in the Klotho/HYP mouse. Endocrinology. 2010; 151(2):492–501. [PubMed: 19952276]
59. Miyagawa K, Yamazaki M, Kawai M, Nishino J, Koshimizu T, Ohata Y, Tachikawa K, Mikuni-Takagaki Y, Kogo M, Ozono K, et al. Dysregulated gene expression in the primary osteoblasts and osteocytes isolated from hypophosphatemic Hyp mice. PLoS One. 2014; 9(4):e93840. [PubMed: 24710520]
60. Smith RC, O'Bryan LM, Farrow EG, Summers LJ, Clinkenbeard EL, Roberts JL, Cass TA, Saha J, Broderick C, Ma YL, et al. Circulating alphaKlotho influences phosphate handling by controlling FGF23 production. J Clin Invest. 2012; 122(12):4710–5. [PubMed: 23187128]
61. Carpenter TO, Imel EA, Ruppe MD, Weber TJ, Klausner MA, Wooddell MM, Kawakami T, Ito T, Zhang X, Humphrey J, et al. Randomized trial of the anti-FGF23 antibody KRN23 in X-linked hypophosphatemia. J Clin Invest. 2014; 124(4):1587–97. [PubMed: 24569459]
62. Imel EA, Zhang X, Ruppe MD, Weber TJ, Klausner MA, Ito T, Vergeire M, Humphrey JS, Glorieux FH, Portale AA, et al. Prolonged Correction of Serum Phosphorus in Adults With X-Linked Hypophosphatemia Using Monthly Doses of KRN23. J Clin Endocrinol Metab. 2015; 100(7):2565–73. [PubMed: 25919461]
63. Aono Y, Shimada T, Yamazaki Y, Hino R, Takeuchi Y, Fujita T, Fukumoto S, Nagano N, Wada M, Yamashita T. The neutralization of FGF-23 ameliorates hypophosphatemia and rickets in Hyp mice. J Bone Miner Metab. 2003; 18(S16)

64. Clinkenbeard EL, Farrow EG, Summers LJ, Cass TA, Roberts JL, Bayt CA, Lahm T, Albrecht M, Allen MR, Peacock M, et al. Neonatal Iron Deficiency Causes Abnormal Phosphate Metabolism by Elevating FGF23 in Normal and ADHR Mice. J Bone Miner Res. 2014; 29(2):361–9. [PubMed: 23873717]

65. Wang X, Wang S, Li C, Gao T, Liu Y, Rangiani A, Sun Y, Hao J, George A, Lu Y, et al. Inactivation of a novel FGF23 regulator, FAM20C, leads to hypophosphatemic rickets in mice. PLoS Genet. 2012; 8(5):e1002708. [PubMed: 22615579]

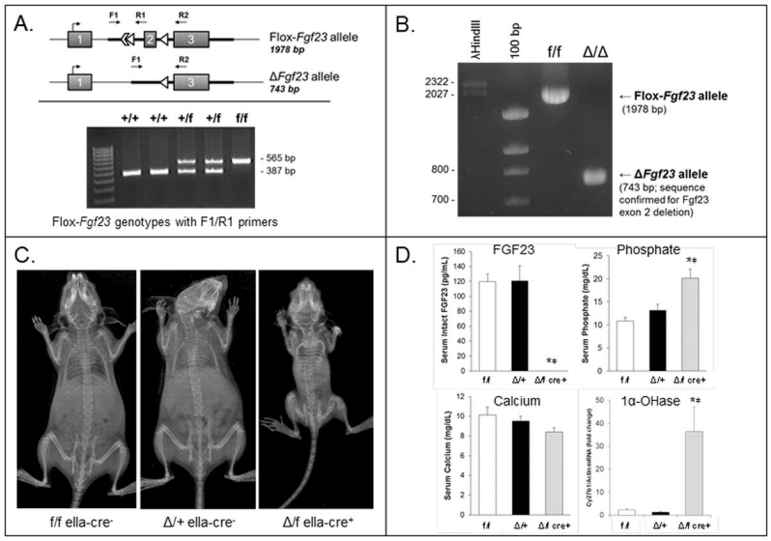

Figure 1. Phenotypes following flox-*Fgf23* recombination

(A) (*upper panel*): Schematic of Flox-*Fgf23* allele showing *Fgf23* exons 1–3, positions of genotyping and sequencing forward (F1) and reverse (R1, R2) PCR primers before (*top*) and after (*bottom*) Cre-mediated recombination; location of LoxP sites surrounding *Fgf23* exon 2 (triangles) and remaining Flp recognition target (FRT) site (open arrowhead) shown; (*lower panel*): Gel electrophoresis of PCR amplification encompassing the proximal LoxP site (primers F1/R1) demonstrated PCR products discernable for wild type ('+/+'), heterozygous ('f/+'), or homozygous ('f/f') flox-*Fgf23* alleles. ***(B)*** PCR amplification of genomic DNA (primers F1/R2) resulted in products of the expected sizes from $Fgf23^{f/f}$ alleles (1978 bp) and the recombined $Fgf23^{\Delta/\Delta}$ alleles (743 bp) (DNA markers are on left, in bp: lambda virus *Hind*III fragments and 100 bp DNA ladder); ***(C)*** Radiographs showed that compared to $Fgf23^{f/f}$ (f/f *eIIa*-cre^{-}) and $Fgf23^{\Delta/+}$ (Δ/+ eIIa-cre^{-}) mice, $Fgf23^{\Delta/f}$/*ella-cre*$^{+}$ (Δ/f ella-cre^{+}) mice were smaller, and had: ***(D)*** undetectable serum FGF23, significantly elevated serum phosphate, similar serum calcium, and elevated kidney vitamin D 1α-OHase (*p<0.05 and ǂp<0.01 vs (f/f) and (Δ/+) respectively, n=3–5 mice per group).

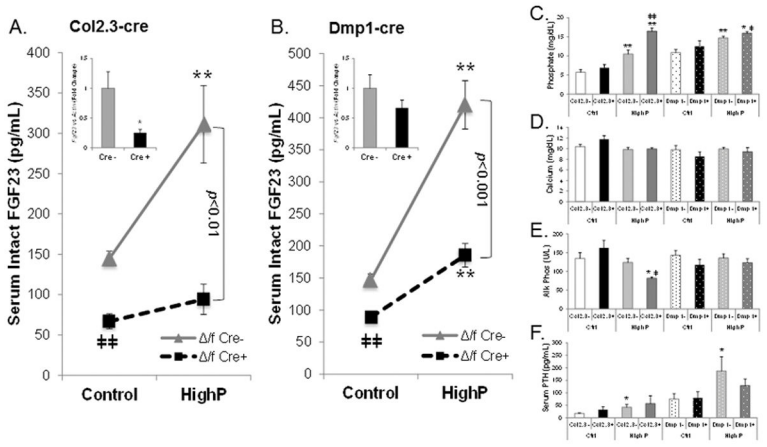

Figure 2. Bone cell-specific targeting of *Fgf23* and responses to phosphate challenge

(A) Serum intact FGF23 was tested in *Fgf23*$^{\Delta/f}$/Col2.3-cre^{-} (Δ/f Cre^{-}) and *Fgf23*$^{\Delta/f}$/Col2.3-cre^{+} (Δ/f Cre^{+}) mice receiving a control or a high phosphate ('HighP') diet. Baseline serum intact FGF23 was reduced in the *Fgf23*$^{\Delta/f}$/Col2.3-cre^{+} mice at 8 weeks, and with 2 week HighP diet challenge was suppressed compared to *Fgf23*$^{\Delta/f}$/Col2.3-cre^{-} mice (**p<0.01 vs control diet same genotype, and ‡‡p<0.01 vs Cre^{-} same diet; n=3–9); (*inset*) Fgf23 mRNA was significantly reduced in *Fgf23*$^{\Delta/f}$/Col2.3-cre^{+} mice versus Cre^{-} controls (*p<0.05); ***(B)*** *Fgf23*$^{\Delta/f}$/Dmp1-cre^{+} mice had lower serum intact FGF23 at 8 weeks of age versus *Fgf23*$^{\Delta/f}$/Dmp1-cre^{-} while receiving control diet; (*inset*) femur Fgf23 mRNA was not statistically different between Cre^{+} or Cre^{-} mice. Following high phosphate diet, the rise of serum intact FGF23 was blunted in *Fgf23*$^{\Delta/f}$/Dmp1-cre^{+} mice (**p<0.01 vs control diet same genotype; ‡‡p<0.01 vs Cre^{-} same diet; n=8–12); ***(C)*** Serum phosphate was elevated in the mice receiving HighP diet, and was significantly higher in *Fgf23*$^{\Delta/f}$/Col2.3-cre^{+} versus all other groups; *Fgf23*$^{\Delta/f}$/Dmp1-cre^{+} mice receiving HighP diet had a trend towards elevated serum phosphate and was significantly different from *Fgf23*$^{\Delta/f}$/Dmp1-cre^{-} mice receiving the HighP diet (*p<0.05 and **p<0.01 vs control diet same genotype, ‡p<0.05 and ‡‡p<0.01 vs Cre- same diet; n=3–12); ***(D)*** Serum calcium was not different across genotypes or diets; ***(E)*** Alkaline phosphatase was reduced in the *Fgf23*$^{\Delta/f}$/Col2.3-cre^{+} mice receiving HighP diet (*p<0.05 vs control diet same genotype; ‡p<0.05 vs Cre^{-} same diet); ***(F)*** Serum intact PTH was elevated in *Fgf23*$^{\Delta/f}$/Col2.3-cre^{-} mice receiving the HighP diet, whereas no change was observed for the *Fgf23*$^{\Delta/f}$/Col2.3-cre^{+} mice. Only the *Fgf23*$^{\Delta/f}$/Dmp1-cre^{-} mice receiving HighP diet had a significant increase in serum PTH (*p<0.05 vs control diet same genotype).

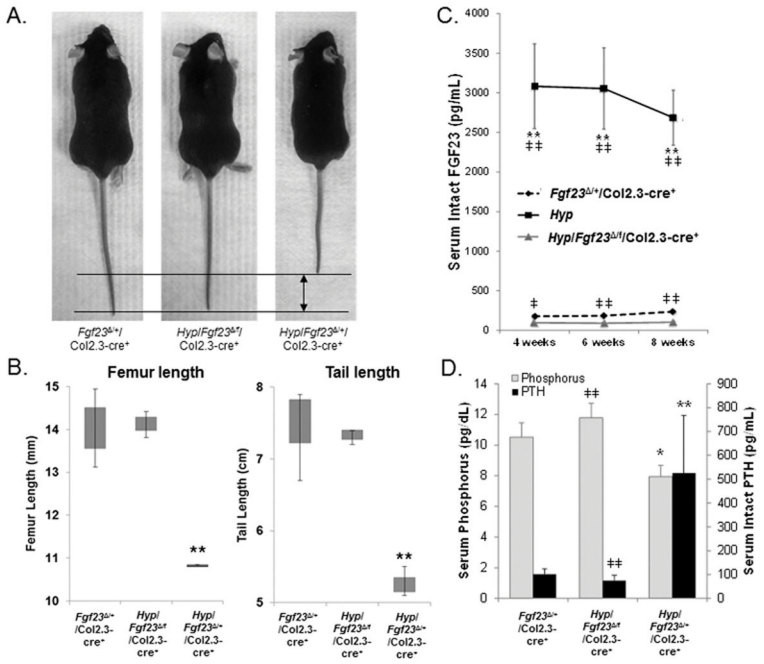

Figure 3. Crossing conditionally-targeted *Fgf23* alleles onto the *Hyp* genetic background

(A) Gross phenotyping showed that the *Hyp*/*Fgf23*$^{\Delta/f}$/Col2.3-cre^{+} were similar to *Fgf23*$^{\Delta/+}$/Col2.3-cre^{+} (phenotypically normal mice) with normal body size and tail length (*arrow*) versus *Hyp* mice; ***(B)*** quantification confirmed *Hyp*/*Fgf23*$^{\Delta/f}$/Col2.3-cre^{+} femur and tail lengths were normalized versus *Hyp* and not different from *Fgf23*$^{\Delta/+}$/Col2.3-cre^{+} mice (n=3–7 males; ***p*<0.01 *Hyp* vs. *Fgf23*$^{\Delta/+}$/Col2.3-cre^{+} and *Hyp*/*Fgf23*$^{\Delta/f}$/Col2.3-cre^{+}); ***(C)*** *Hyp*/*Fgf23*$^{\Delta/f}$/Col2.3-cre^{+} mice had significantly reduced basal intact serum FGF23 versus *Fgf23*$^{\Delta/+}$/Col2.3-cre^{+} and *Hyp* from weaning to 8 weeks of age (***p*<0.01 vs *Fgf23*$^{\Delta/+}$/Col2.3-cre^{+}; ‡*p*<0.05, ‡‡*p*<0.01 vs *Hyp*/*Fgf23*$^{\Delta/f}$/Col2.3-cre^{+}; n=5–9); ***(D)*** Serum phosphate in *Hyp*/*Fgf23*$^{\Delta/f}$/Col2.3-cre^{+} mice was corrected compared to the hypophosphatemia in *Hyp* and not different from *Fgf23*$^{\Delta/+}$/Col2.3-cre^{+} mice. Additionally, serum PTH was highly elevated in *Hyp* compared to *Fgf23*$^{\Delta/+}$/Col2.3-cre^{+} mice. These levels were corrected in the *Hyp*/*Fgf23*$^{\Delta/f}$/Col2.3-cre^{+} mice (**p*<0.05, ***p*<0.01 vs *Fgf23*$^{\Delta/+}$/Col2.3-cre^{+}, ‡‡*p*<0.01 vs *Hyp*; n=7–9).

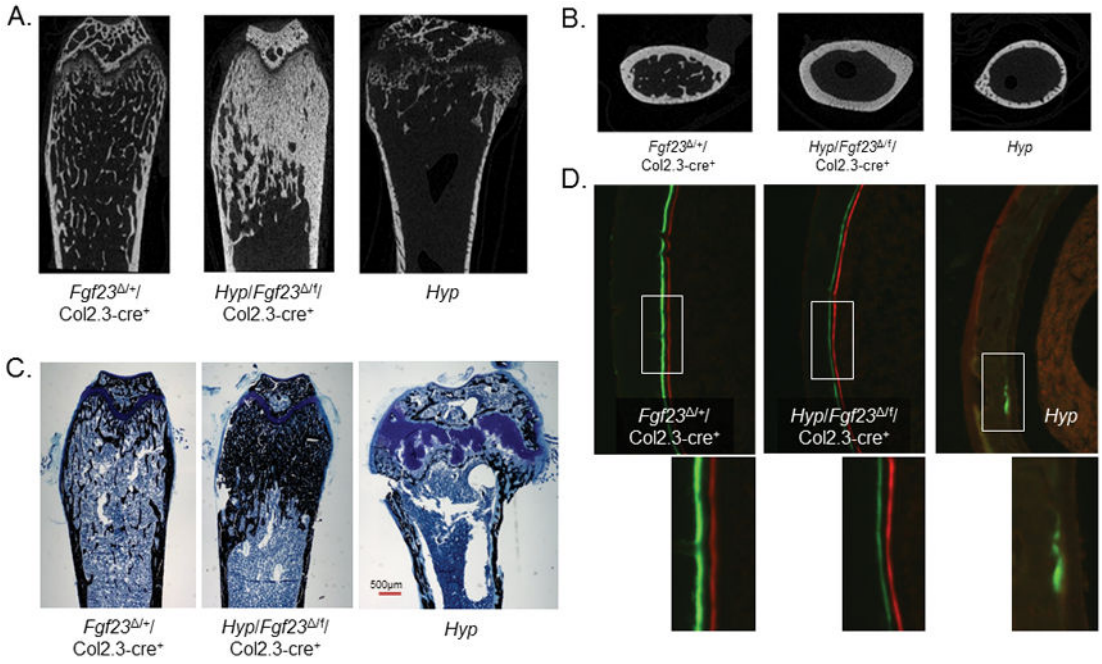

Figure 4. Skeletal μCT and histomorphometry of *Hyp*/*Fgf23*$^{\Delta/f}$/Col2.3-cre^{+} mice

(A) As assessed by μCT, compared to *Fgf23*$^{\Delta/+}$/Col2.3-cre^{+} mice the metaphyses of *Hyp*/*Fgf23*$^{\Delta/f}$/Col2.3-cre^{+} lacked marrow space or trabeculae definition due to the abundant bone. *Hyp* mice had lack of trabecular bone and misshapen femoral head. **(*B*)** Mid-diaphysis images showed reduced porosity and higher bone area relative to total area in *Hyp*/*Fgf23*$^{\Delta/f}$/Col2.3-cre^{+} versus *Hyp*; ***(C)*** Von Kossa staining of femora qualitatively revealed that *Hyp*/*Fgf23*$^{\Delta/f}$/Col2.3-cre^{+} mice had resolved the *Hyp* widened growth plate, distended bone, and osteomalacia characteristic of this model; and ***(D)*** Histomorphometry demonstrated *Hyp*/*Fgf23*$^{\Delta/f}$/Col2.3-cre^{+} bone had dynamic bone formation rates similar to *Fgf23*$^{\Delta/+}$/Col2.3-cre^{+} as determined by dual fluorescence labeling whereas *Hyp* mice had virtually no label uptake (*upper panels*). Enlarged regions of label are boxed and shown beneath their respective genotypes (*lower panels*).

Table 1

µCT and histomorphometric analyses.

	***Fgf23*$^{\Delta/+}$/Col2.3-cre^{+}**	***Hyp*/*Fgf23*$^{\Delta/f}$/Col2.3-cre^{+}**	***Hyp***
µCT			
Cancellous BV/TV, %	16.2 ± 1.3***	76.6 ± 8.4*** ╪╪╪	2.8 ± 0.9
Cortical BA/TA, %	43 ± 1**	40 ± 1**	27 ± 1
Cortical porosity, %	0.06 ± 0.02*	0.48 ± 0.2*	11 ± 5
Cortical thickness, mm	0.16 ± 0.01**	0.15 ± 0.01**	0.08 ± 0.01
Dynamic Histomorphometry			
Periosteal MS/BS, %	66 ± 6**	82 ± 6**	18 ± 7
Periosteal MAR, um/day	2.7 ± 0.2**	3.5± 0.4**	0.5 ± 0.5
Periosetal BFR/BS, um^3/um^2/year	667 ± 83**	1035 ± 106** ╪	76 ± 76
Endocortical MS/BS, %	60 ± 7**	74 ± 5**	15 ± 6
Endocortical MAR, um/day	2.1 ± 0.2**	2.4 ± 0.1**	*ND*
Endocortical BFR/BS, um^3/um^2/year	409 ± 97**	538 ± 70**	*ND*

Data presented as mean and standard error (*p<0.05 **p<0.01 and ***p<0.001 vs *Hyp*, ╪p<0.05 ╪╪p<0.01 and ╪╪╪p<0.001 vs $Fgf23^{\Delta/+}$/Col2.3-cre+). BV, bone volume; TV, total volume; BA, bone area; TA, total area; MS/BS, mineralizing surface per bone surface; MAR, mineral apposition rate; BFR/BS, bone formation rate per bone surface. '*ND*' is not detectable with reference to the lack of sufficient label uptake within the specimens; these were designated as '0' for statistical purposes.